

We are IntechOpen, the world's leading publisher of Open Access books Built by scientists, for scientists

6,900

Open access books available

186,000

International authors and editors

200M

Downloads

Our authors are among the

154

Countries delivered to

TOP 1%

most cited scientists

12.2%

Contributors from top 500 universities



WEB OF SCIENCE™

Selection of our books indexed in the Book Citation Index
in Web of Science™ Core Collection (BKCI)

Interested in publishing with us?
Contact book.department@intechopen.com

Numbers displayed above are based on latest data collected.
For more information visit www.intechopen.com



Tracking Control of Unmanned Aerial Vehicle for Power Line Inspection

*Kenta Takaya, Hiroshi Ohta, Keishi Shibayama
and Valeri Kroumov*

Abstract

This work presents some results about power transmission line tracking control and a full autonomous inspection using a quadrotor helicopter. The presented in this paper power line autonomous inspection allows detecting power line defects caused by thunderstorms, corrosion, insulator malfunctions, and same time monitoring of vegetation under the power line corridor. Traditional inspection is performed by helicopters equipped with high-resolution cameras or by direct visual examination carried out by highly skilled staff climbing over de-energized power lines. However, the visual inspection is time-expensive and costly. Moreover, due to regulatory constraints, the helicopters cannot cover narrow mountainous areas. Unmanned aerial vehicles (UAV) are an attractive alternative for power line inspection. In this work, a mathematical model for the quadrotor helicopter used in the autonomous inspection is presented. The model is successfully evaluated through simulations and flight experiments. Next, the construction of a quadrotor helicopter system and its application to power line autonomous inspection is introduced. Simulation and experimental results demonstrate the efficiency and applicability of that system. The results of this research are in the process of implementation for regular inspection of electrical transmission lines.

Keywords: power line tracking, UAV navigation, power line inspection, quadrotor helicopter, field robotics

1. Introduction

Electric power companies worldwide are obliged to guarantee disruptive electrical power supply. The power transmission facilities mainly include power lines, towers, and insulators. These facilities are exposed to thunderstorms, thermal deviations, ice, rain, pollutions like volcanic gases and sour rains: a severe environment that may lead to material fatigue, oxidation, and corrosion. Electric companies are required to inspect and maintain the power transmission equipment periodically. Ground patrols partially inspect these facilities, and, as shown in **Figure 1**, direct visual examination is carried out by skilled personnel climbing over de-energized power lines. As yet, visual inspection is time-expensive and labour-intensive. A common approach nowadays is to use helicopters equipped with high-resolution cameras, but in such inspection, helicopters cannot cover narrow mountainous

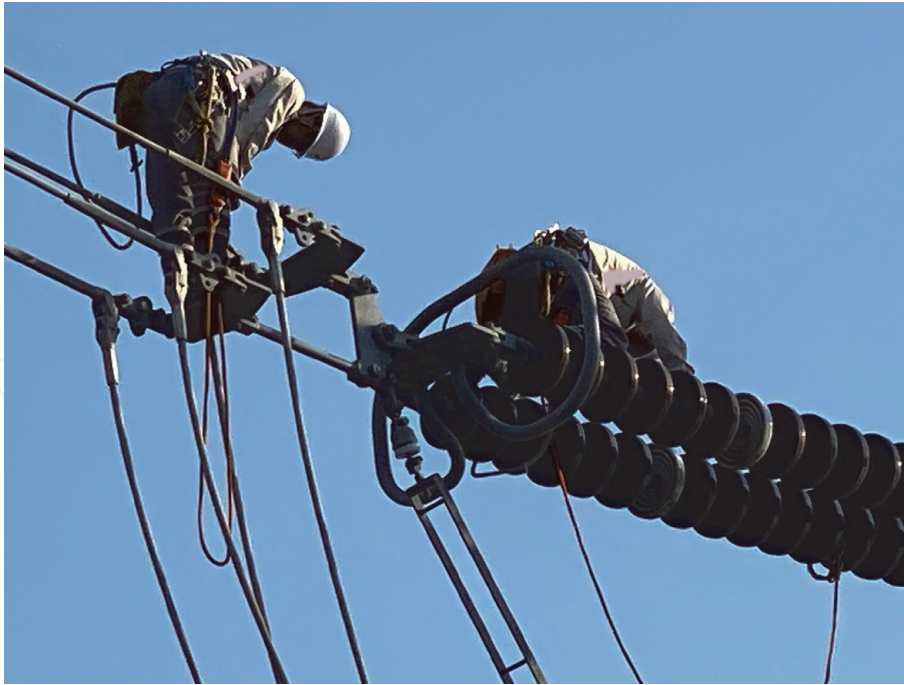


Figure 1.
Power line inspection works.

regions due to regulatory constraints. According to the Statistical Report of the Federation of Electric Power Companies in Japan, the total length of high voltage power transmission lines in the country in 2010 is more than 100,000 km, and the number of power transmission towers is much more than 220,000 [1]. Most power transmission facilities in Japan are situated in mountainous regions with no ordinary roads, making the inspection time-consuming and costly.

Unmanned aerial vehicles (UAV) are a promising solution for power line inspection because of time and cost efficiency and because UAVs can approach and inspect energized lines safely. Hence, a significant amount of research is addressing this field. Many researchers have applied computer vision techniques for power transmission towers, and insulators recognition [2–8]. Image processing algorithms are also heavily employed to power lines recognition and tracking [2, 9–17]. However, in most of these studies, distance to the lines is not measured, and their robustness is challenging. In [2] a Region-Based Convolutional Neural Network (R-CNN) is used to localization of transmission towers, and their UAV navigation relies on real-time image processing. The authors of [2] claim that “It is the first time to navigate UAV simultaneously utilizing transmission towers and lines”. In [9, 15] after the quadrotor helicopter is navigated to the start point of inspection manually, the vehicle performs autonomous waypoint flight above power lines. Additionally, a Light Detection and Ranging (LiDAR) sensor detect and reconstruct the power line shape [15]. Nevertheless, such navigation may be applied to power distribution lines, but manual flight cannot be performed safely enough when there is a substantial distance to the inspection object. In [11] power transmission lines situated in a highly-populated area are successfully tracked in waypoint flight mode with an aerial speed of 8 m/s. Similar algorithms for power transmission line tracking using position-based visual servo controllers are developed in [10, 12, 13] and are evaluated through several simulations. In [16] an image-based visual servoing combined with a linear quadratic servo control is developed. Deep reinforcement learning is quite successfully applied to autonomous line tracking in [18]. However, network training is performed within a simulation environment, and the robustness of that approach in the real world remains a challenge. The distance to the power line in [18] is measured using a depth camera or stereo camera.

Because of the great significance of automated power lines inspection, power supply companies are rigorously approaching the problem, too [19–23]. However, as far as we know, UAVs are not yet deployed to inspect power line transmission facilities. Hydro-Québec [19] is developing a robot called LineRanger to inspect transmission line conductor bundles. The robot is directly attached to the power line bundle and automatically crosses obstacles like line separators and suspension insulators. LineRanger is equipped with a high-resolution camera and a LiDAR for vegetation monitoring. The system can cover several kilometers a day. They have also developed a similar robotic system called LineScout, capable of inspecting a single transmission line [20]. It can acquire visual information and measure the joints' electrical resistance and monitor the corrosion level of the conductors. DJI M200 Series drones produced by DJI are effectively deployed for power line inspection mainly under manual operation [21]. Although manual vehicle guidance is not time-effective, such inspection is much better than the direct one. The University of KwaZulu-Natal is working with Eskom Holdings SOC Ltd. to develop a power line inspection robot [22], which can climb around jumpers and suspension clamps on a single power transmission line or ground wire. The Electric Power Research Institute (EPRI) is developing a transmission line inspection robot [23], known as “Ti,” that can be permanently installed to traverse about 130 km of transmission lines. The robot can transmit in real-time weather data, vegetation imaging, and detect any obstructions on lines. EPRI also worked with manufacturer RADĒCO Inc. and Exyn Technologies to develop “an autonomous drone to inspect components in elevated hard-to-access areas, search for temperature anomalies, and collect dose rate surveys in radiological zones” [24]. With UAV's Level 4 technology, the UAV can perform a free-flight exploration of complex spaces while collecting data from the environment [25, 26]. This technology will speed up the implementation of UAVs in the autonomous inspection.

This work presents a novel quadrotor-based system for power line inspection. An outline and some preliminary results of this research are presented in [27], but this paper describes the power line tracking algorithm and its effectiveness and applicability. The main contributions of this study are (1) the development of a quadrotor based system for autonomous inspection of electrical energy transmission and distribution assets. The presented in this paper system has almost Level 4 autonomy in the sense that it can perform flights beyond visual line of sight and without operator based navigation. (2) As far as we are concerned, this is the first time a quadrotor UAV is used in a real application for full autonomous inspection of power lines. (3) The developed system can be applied to almost any industrial multirotor helicopter able to carry the payload of sensors and cameras necessary for inspection.

The rest of the paper is organized as follows. Section 2 presents the quadrotor model used in this development. Section 3 describes the hardware and software configuration of the quadrotor system briefly. The quadrotor model described in Section 2 is evaluated in Section 4 and simulation and experimental results demonstrating the usability of the developed tracking system are depicted there. The last section concludes the paper and gives some plans for further expansion of this work.

2. Quadrotor helicopter dynamics and control

2.1 Quadrotor dynamics

The quadrotor configuration and its reference coordinate systems are shown in **Figure 2**. The vehicle model is acquired under the following assumptions:

1. The quadrotor construction is rigid and symmetrical.
2. The propellers are rigid.
3. The ground effect is neglected, and the centre of gravity of the vehicle lies at the origin of its body coordinate system.

The world reference frame is O_n and the body fixed frame is O_b . The x_b axis of body frame points at normal flight direction, y_b is in starboard side, and z_b axis is in descend direction. The absolute position of the quadrotor body frame $\mathbf{p}^n = [x_n \ y_n \ z_n]^T$ is given by three coordinates of the center of mass in O_n , and its attitude is given by three Euler angles $\mathbf{r}^b = [\phi \ \theta \ \psi]^T$ standing for roll, pitch and yaw angles, respectively.

The dynamics of the quadrotor helicopter expressed in Newton–Euler notation [28–31] as:

$$\dot{\mathbf{p}}^n = \mathbf{v}^n \quad (1)$$

$$\dot{\mathbf{v}}^n = m^{-1} \mathbf{C}_b^n \mathbf{F}_b \quad (2)$$

$$\dot{\mathbf{r}}^b = \boldsymbol{\omega}^b \quad (3)$$

$$\dot{\boldsymbol{\omega}}^b = \mathbf{J}^{-1} \mathbf{M}_b + \mathbf{J}^{-1} (\boldsymbol{\omega}^b \times \mathbf{J} \boldsymbol{\omega}^b), \quad (4)$$

where m is the mass of the quadrotor frame and \mathbf{C}_b^n is the rotation matrix to transform the body frame into world reference frame O_n . The quadrotor translational and rotational motions control is performed by properly changing the thrust F_{T_i} , $i = 1, \dots, 4$ of rotors. The thrust of the rotors varies by changing their angular speed. The rotor thrust is proportional to the square of the angular rotor speed:

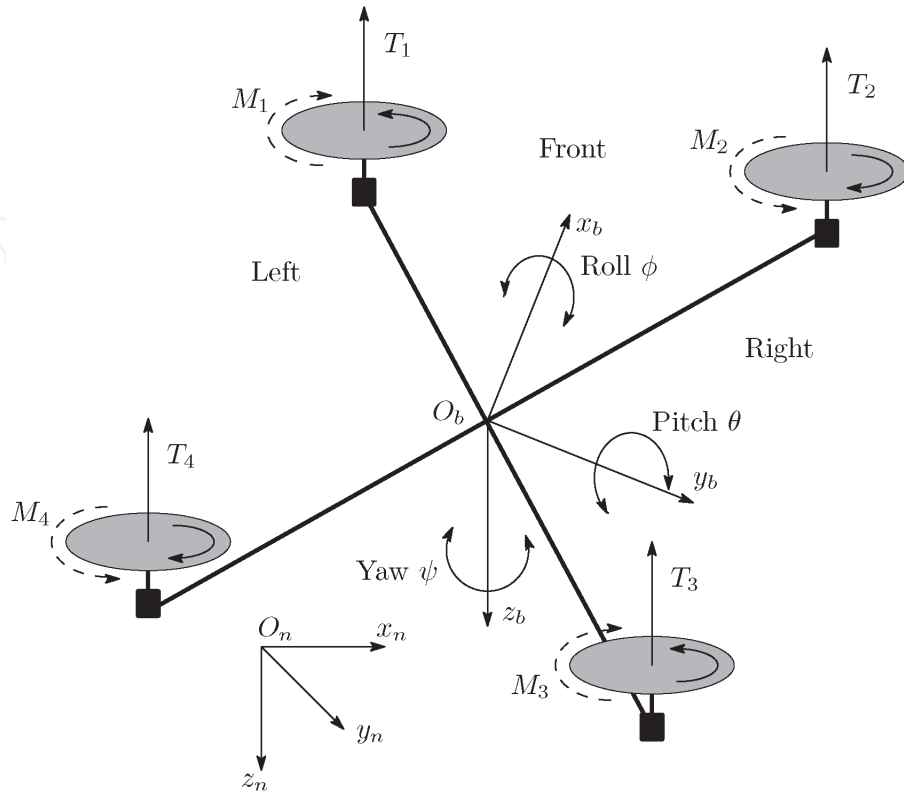


Figure 2.
Quadrotor UAV body and world coordinate systems.

$$F_{T_i} = C_T \omega_{m_i}^2, \quad (5)$$

where C_T is a thrust coefficient, and the angular speed of the rotor is [28]:

$$\dot{\omega}_{m_i} = \frac{1}{J_m} \left(\frac{k_e}{R_m} (U_i - k_e \omega_{m_i}) - (k_t F_{T_i} + D \omega_{m_i}) \right), \quad i = 1, \dots, 4, \quad (6)$$

where U_i is the voltage applied to the motor, J_m is the moment of inertia of the armature and the propeller, R_m is the resistance of the armature coil, k_e and k_t are the electromotive force and torque constants, respectively, and D is the motor viscous friction constant.

The torque generated by the motor i is:

$$M_i = k_t F_{T_i} = k_t C_T \omega_{m_i}^2. \quad (7)$$

The total thrust F_z is:

$$F_z = \sum_{i=1}^4 F_{T_i}, \quad (8)$$

and control torque vector produced by the four motors is:

$$\mathbf{M} = \begin{bmatrix} M_x \\ M_y \\ M_z \end{bmatrix} = \begin{bmatrix} ((F_{T_1} + F_{T_4}) - (F_{T_2} + F_{T_3})) l_m / \sqrt{2} \\ ((F_{T_1} + F_{T_2}) - (F_{T_3} + F_{T_4})) l_m / \sqrt{2} \\ -M_1 + M_2 - M_3 + M_4 \end{bmatrix}. \quad (9)$$

The propeller gyro moments in roll and yaw directions are:

$$M_{jx} = -J_r \omega_r \dot{\theta} \quad (10)$$

$$M_{jy} = J_r \omega_r \dot{\psi} \quad (11)$$

where J_r is the rotor inertia and $\omega_r = \omega_{m_1} - \omega_{m_2} + \omega_{m_3} - \omega_{m_4}$.

The gravitational force in z direction is:

$$\mathbf{F}_g = m \mathbf{C}_b^n [0 \quad 0 \quad g]^T. \quad (12)$$

The drag reluctant force is a result of the air friction during vehicle movement and rotation:

$$\mathbf{F}_d = C_{d,F} |\mathbf{v}^b| \mathbf{v}^b \quad (13)$$

$$\mathbf{M}_d = C_{d,M} |\boldsymbol{\omega}^b| \boldsymbol{\omega}^b \quad (14)$$

where, $C_{d,F}$ and $C_{d,M}$ are aerodynamic coefficient matrices:

$$\begin{aligned} C_{d,F} &= \text{diag} [C_{d,F_x} \quad C_{d,F_y} \quad C_{d,F_z}] \\ C_{d,M} &= \text{diag} [C_{d,M_x} \quad C_{d,M_y} \quad C_{d,M_z}]. \end{aligned} \quad (15)$$

The drag generated by the lateral wind is proportional to square of the wind speed:

$$F_w = C_{d,F} |v_w| v_w. \quad (16)$$

The speed dynamics is expressed as:

$$\begin{bmatrix} \dot{v}_x^b \\ \dot{v}_y^b \\ \dot{v}_z^b \end{bmatrix} = \frac{1}{m} \begin{bmatrix} (S\phi S\psi - C\phi S\theta C\psi)F_z - F_{d,x} - F_{w,x} \\ (S\phi C\psi + C\phi S\theta S\psi)F_z - F_{d,y} - F_{w,y} \\ mg - C\phi C\theta F_z - F_{d,z} - F_{w,z} \end{bmatrix}, \quad (17)$$

where C and S stand for sin and cos functions.

Now, for simplicity the gyro angular moment and vehicle angular moment are included in disturbance vector M_d :

$$\begin{bmatrix} \ddot{\phi} \\ \ddot{\theta} \\ \ddot{\psi} \end{bmatrix} = \begin{bmatrix} J_x^{-1}(M_x - M_{d,x}) \\ J_y^{-1}(M_y - M_{d,y}) \\ J_z^{-1}(M_z - M_{d,z}) \end{bmatrix} \quad (18)$$

Finally, the vehicle dynamics, including the motor models, become [28, 30, 32]:

$$\begin{aligned} \dot{x} &= v_x^b \\ \dot{y} &= v_y^b \\ \dot{z} &= v_z^b \\ \ddot{x} &= m^{-1}((S\phi S\psi - C\phi S\theta C\psi)F_z - F_{d,x} - F_{w,x}) \\ \ddot{y} &= m^{-1}((S\phi S\psi - C\phi S\theta C\psi)F_z - F_{d,y} - F_{w,y}) \\ \ddot{z} &= m^{-1}((mg - C\phi C\theta)F_z - F_{d,z} - F_{w,z}) \\ \dot{\phi} &= \omega_x \\ \dot{\theta} &= \omega_y \\ \dot{\psi} &= \omega_z \\ \ddot{\phi} &= J_x^{-1}(((F_{T_1} + F_{T_4}) - (F_{T_2} + F_{T_3}))L_M/\sqrt{2} - M_{d,x}) \\ \ddot{\theta} &= J_y^{-1}(((F_{T_1} + F_{T_4}) - (F_{T_2} + F_{T_3}))L_M/\sqrt{2} - M_{d,y}) \\ \ddot{\psi} &= J_z^{-1}((-M_1 + M_2 - M_3 + M_4) - M_{d,z}) \\ \dot{\omega}_{m_1} &= J_m^{-1}\left(\frac{k_e}{R_m}(U_1 - k_e\omega_{m_1}) - k_t F_{T_1}\right) \\ \dot{\omega}_{m_2} &= J_m^{-1}\left(\frac{k_e}{R_m}(U_2 - k_e\omega_{m_2}) - k_t F_{T_2}\right) \\ \dot{\omega}_{m_3} &= J_m^{-1}\left(\frac{k_e}{R_m}(U_3 - k_e\omega_{m_3}) - k_t F_{T_3}\right) \\ \dot{\omega}_{m_4} &= J_m^{-1}\left(\frac{k_e}{R_m}(U_4 - k_e\omega_{m_4}) - k_t F_{T_4}\right), \end{aligned} \quad (19)$$

where the viscous friction D in (6) is neglected. The frame control inputs become the motor drive voltages U_i .

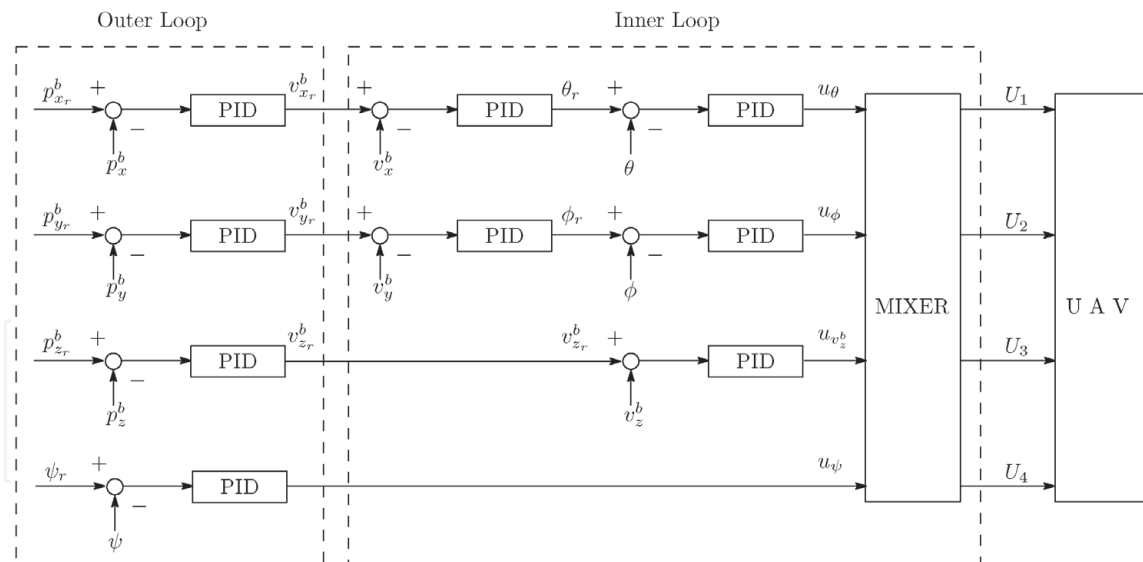


Figure 3.
 Quadrotor helicopter cascaded PID control system.

2.2 Control scheme

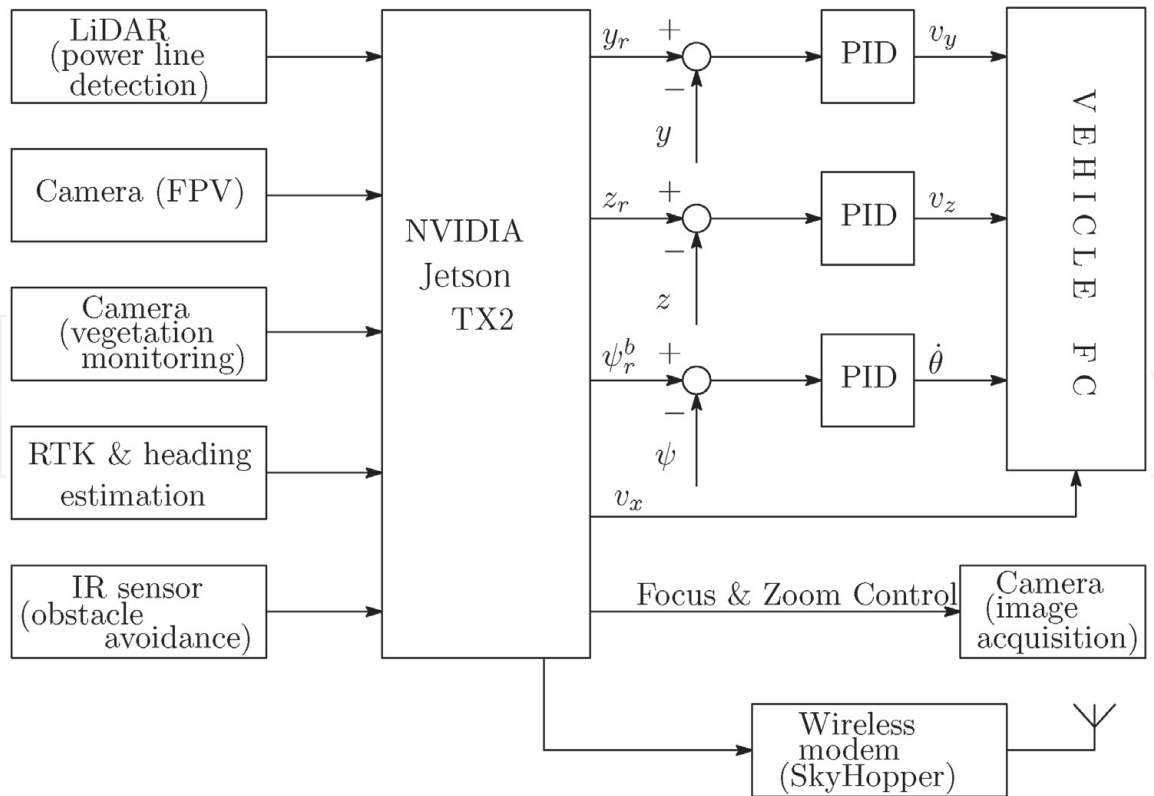
The overall structure of the closed-loop control of the quadrotor frame is shown in **Figure 3**. The vehicle is an underactuated mechanical system with six degrees of freedom and only four control inputs. The controller consists of a set of cascaded PID controllers arranged in inner and outer loops. The inner loops control the attitude, yaw rate, and vertical velocity. The outer loop controls the altitude and heading. Both loops are designed similarly to those implemented in the actual quadrotor flight controller [33]. This control technique is called a time-scale separation [34] and works well when the inner loops are significantly faster than the outer ones. The MIXER block in **Figure 3** forms the voltages applied to the motors:

$$\begin{aligned}
 U_1 &= -u_\phi + u_\theta - u_\psi + u_{v_z^b} \\
 U_2 &= u_\phi + u_\theta + u_\psi + u_{v_z^b} \\
 U_3 &= u_\phi - u_\theta - u_\psi + u_{v_z^b} \\
 U_4 &= -u_\phi - u_\theta + u_\psi + u_{v_z^b}.
 \end{aligned} \tag{20}$$

3. Power line autonomous inspection system architecture

3.1 Hardware design

The hardware architecture of the quadrotor system is shown in **Figure 4a**. The power transmission lines are detected using a LiDAR pointing in a vertical direction. Measured distance to the power line by the same LiDAR is used to adjust the zoom and focus of the image acquisition camera. The obstacle avoidance algorithm uses an infrared Time-of-Flight (ToF) sensor having 360° range and pointing horizontally. Because the magnetic field generated by the power lines interferes with the internal compass of the flight controller, the heading of the vehicle is estimated through a moving baseline real-time kinematics (RTK) [35] technique. For safety reasons, a second GNSS module is added to the frame. A second camera pointing in the down direction performs the vegetation monitoring under the power line corridor. All sensors are connected to NVIDIA Jetson TX2 [36] companion computer, which controls the position of the vehicle via MAVLink protocol [37]. The real-time



(a)



(b)

Figure 4. Hardware architecture and vehicle appearance. (a) Hardware architecture, (b) appearance of the quadrotor system.

images from a first-person view (FPV) camera and the complete status of the quadrotor (position in the world and the local coordinate systems, battery level, GNSS status, magnetic field strength) are transmitted to the ground station computer in 1 s intervals for system monitoring. The wireless modem (SkyHopper PRO V [38]) performs all necessary communications between the quadrotor frame and the ground station. The aircraft is stabilized by a Pixhawk flight controller (FC) [39]. However, the altitude z^b and lateral control x^b during line tracking is

Parameter	Value
Propeller diameter [in]	19
Maximum payload [kg]	2.0
Weight [kg]	6.5
Flight time [min]	20
LiDAR resolution [deg]	0.125
RTK module	Yes
Companion computer	Jetson TX2 [36]
Wireless modem	SkyHopper PRO V [38]
Flight controller	Pixhawk [39]

Table 1.
 Quadrotor vehicle specifications.

performed using three outer loops realized on the companion computer as shown in **Figure 4a**. FC controls the forward speed with a reference command from the companion computer. The vision system estimates the yaw angle ψ . **Figure 4b** depicts the UAV appearance. The specifications of the quadrotor helicopter are given in **Table 1**.

3.2 Software

The control software is realized in Python language, and most of it runs under Robot Operating System (ROS) [40]. The software consists of modules for sensor data acquisition and processing, camera control node, and node for sensor data transmission to the control process and the same time to the base station computer. The control process receives power line position measured by the LiDAR pointing in the down position in the body coordinate system, GNSS coordinates of the tower to be inspected, GNSS receiver status, battery status, and FC status. The control process uses three PID controllers for altitude and yaw control, as shown in **Figure 4a**. It performs path generation as well as almost all necessary processing for realizing a safe flight.

Even though the vehicle control software communicates with the sensor relating nodes, it runs thoroughly independent from the ROS processes for safety reasons. Because of this autonomy, the control process can bring the vehicle safely back to the home position even if the whole ROS crashes or all sensors except one of the GPS modules get out of order.

3.3 Power line tracking

The inspection process includes the following actions. As shown in **Figure 5**, after taking off at safe altitude, the vehicle approaches the start tower of the inspection path using *a priori* information about the tower world coordinates and its height. Then the electrical line subject to inspection is detected by the LiDAR pointing in a downward direction. Next, the vehicle is positioned above the wire at a distance allowing it to acquire good quality images. While keeping a constant distance to the power line, the quadrotor moves along it at a constant speed and acquires high-resolution images of the wire and the vegetation below. After reaching the last tower subject of inspection, the quadrotor returns safely to the home position.

The autonomous inspection consists of the following steps:

1. Selection of the inspection target using a graphical user interface (GUI) running on the base station computer (see **Figure 6**).
2. Using a priori data about the tower position in the world coordinate system and its mechanical construction, the vehicle takes off to a safe altitude. It approaches the top of the tower using GNSS measurements.

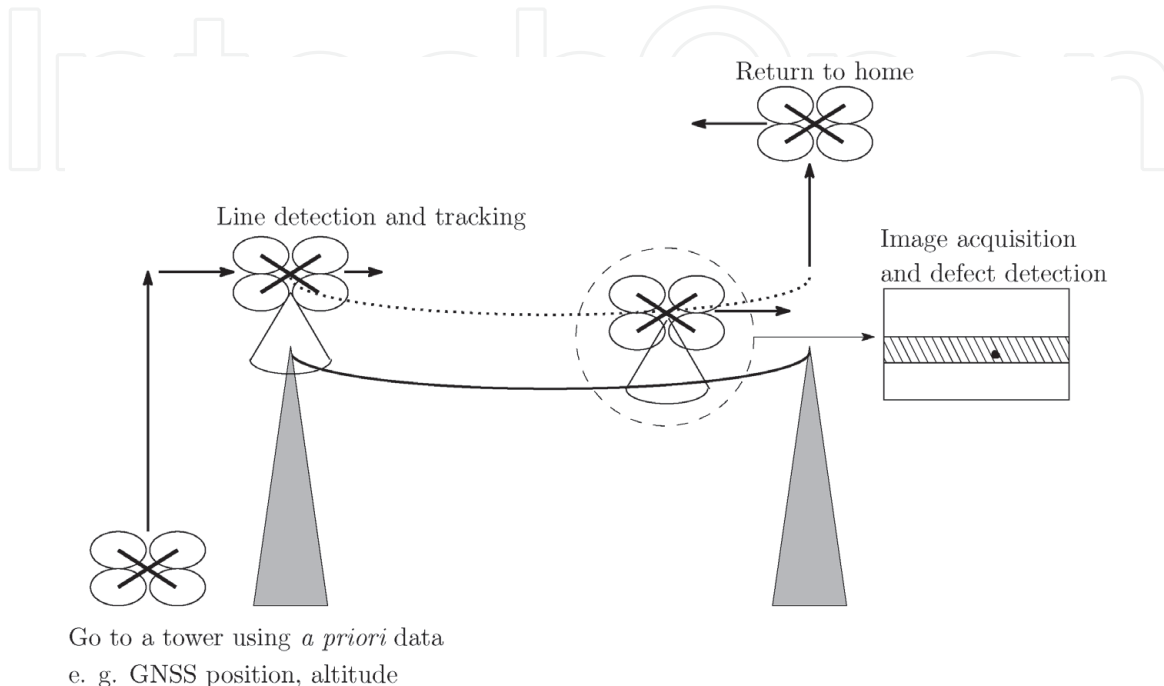


Figure 5.
Power line tracking concept.

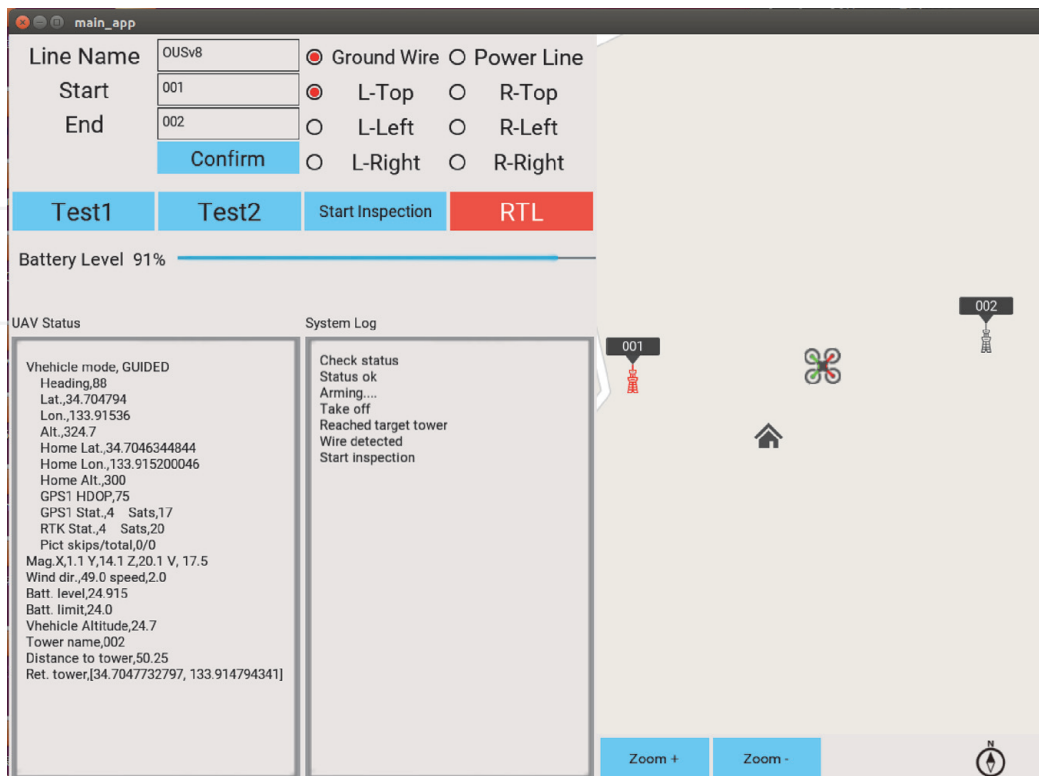


Figure 6.
GUI for power line inspection. GW: ground wire, L: left, R: right, RTL: return to launch.



Figure 7.
Quadrotor system during power line autonomous inspection.

3. Search of the power line subject of the inspection. The search is performed using LiDAR readings of the power line position.
4. Power line tracking control at a certain velocity and constant distance, based on the LiDAR measurements and same time performing continuous image acquisition and image processing for detection of rust and defects on the power line. An additional camera monitors the vegetation under the power line corridor.
5. After finishing the inspection, the UAV returns safely back to the home position.

The GUI is used to send the inspection subject to the quadrotor companion computer before the beginning of the inspection. It also displays the UAV status during the flight and its position on the map. The power transmission towers are displayed on the same map, too. Preflight safety tests of the vehicle and the control software can also be invoked from the same GUI. After the beginning of the inspection, communication from the aircraft only is performed. Only the Return to Launch (RTL) command can be transmitted from the GUI.

The GUI in **Figure 6** shows a setting for a ground wire (GW) inspection. Images of the ground wire can be acquired from above and from a slant direction. The subject shown in the figure is a transmission tower with two ground wires. The left-side wire is selected, and the images from the top above are to be acquired. Left or right side GWs can also be inspected from slant direction: “R-Left” means right-side wire to be scanned from the left-side, “R-Right” means right-side wire to be scanned from the right-side and so on.

Figure 7 shows the UAV during autonomous ground wire inspection. The image in **Figure 7** is acquired by a camera mounted on a second aircraft.

4. Simulation and experimental results

4.1 Step response simulation and experiments

In this section, the quadrotor model (Eq. (19)) is validated by simulation and experiments. The UAV specification is shown in **Table 1**. The parameters of the

quadrotor are shown in **Table 2** and PID controller parameters are depicted in **Table 3**. In these experiments, the model and actual vehicle are moved along body coordinates system axes at a constant speed. The simulation and experimental responses are compared in **Figure 8**. **Figure 8a, c, and e** show the responses during up-down, forward-backward, and left-right flights. The simulation and experimental results are very similar, showing that the model presents the actual vehicle's behavior well. It can be seen that the actual vehicle in up-down flights tends to increase the altitude slightly, and we suppose that might exist some problem in tuning the flight controller filter parameters, causing error in the estimation of the

Parameter	Value	Description
U [V]	25.0	Maximum input voltage
R_m [Ω]	0.013	Armature resistance
k_e [s/rad]	0.0306	Back EMF coefficient
k_t	1.0×10^{-4}	Torque coefficient
J_m [kg·m ²]	6.68×10^{-4}	Rotor moment of inertia
C_{T0} [N/rad ²]	3.37×10^{-5}	Thrust coefficient
m [kg]	7.0	Total weight
l_m [m]	0.275	Motor distance to the center of UAV
J_x [kg·m ²]	0.637	Moment of inertia (x-axis)
J_y [kg·m ²]	0.637	Moment of inertia (y-axis)
J_z [kg·m ²]	0.52	Moment of inertia (z-axis)
C_{d,F_x}	0.167	Drag coefficient (x-axis)
C_{d,F_y}	0.167	Drag coefficient (y-axis)
C_{d,F_z}	0.059	Drag coefficient (z-axis)
C_{d,M_x}	0.059	Rotational drag coefficient (x-axis)
C_{d,M_y}	0.059	Rotational drag coefficient (y-axis)
C_{d,M_z}	0.167	Rotational drag coefficient (z-axis)

Table 2.
UAV parameters.

Controller	P	I	D
Speed v_x^b	0.225	0.225	0.02
Speed v_y^b	0.225	0.225	0.02
Speed v_z^b	25.0	5.0	0.0
Roll ϕ	70.0	25.0	10.0
Pitch θ	70.0	25.0	10.0
Yaw ψ	100.0	3.5	150
Position y^b	0.15	0.0	0.05
Position z^b	0.5	0.03	0.05

Table 3.
PID controllers parameters.

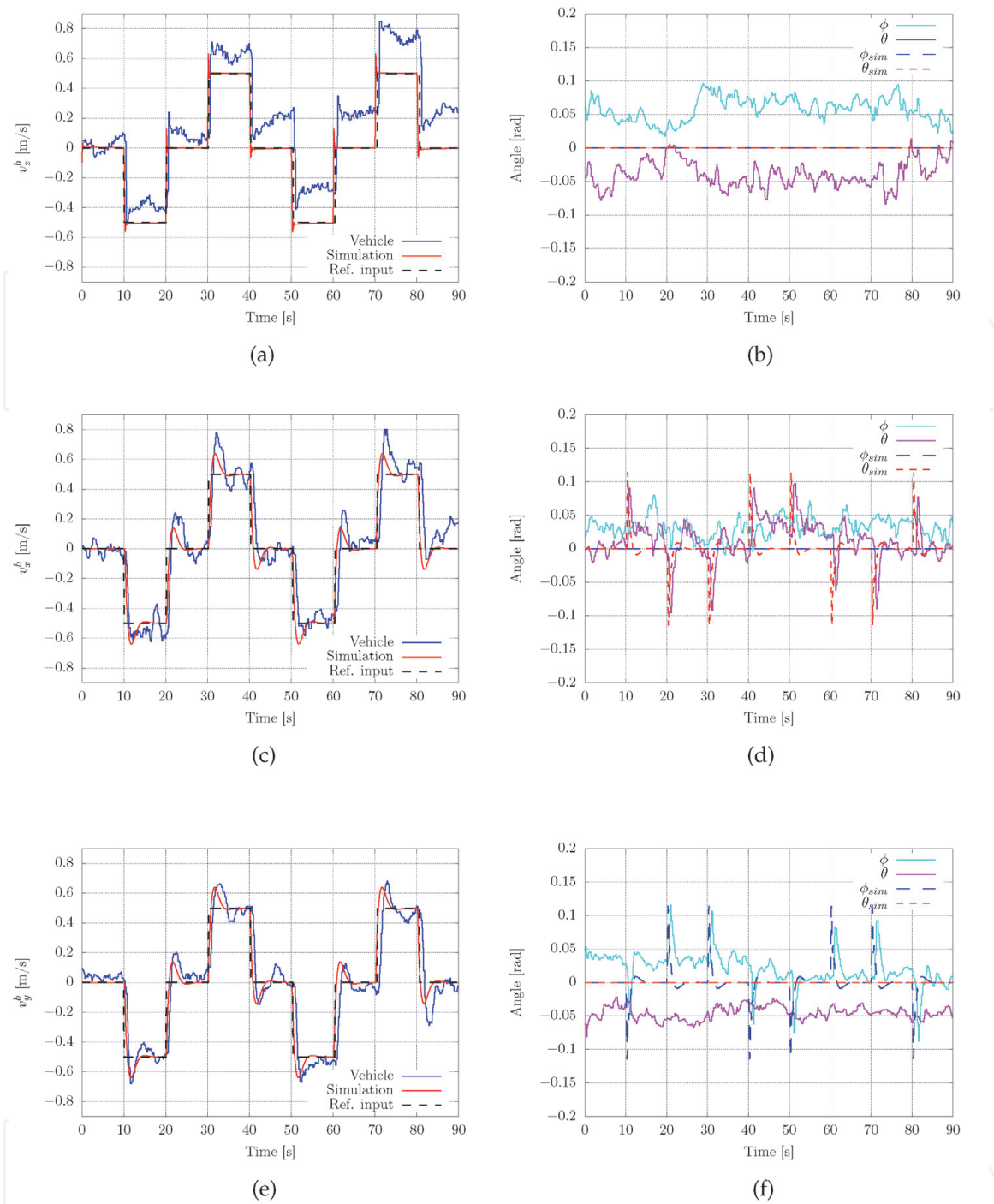


Figure 8. Step response simulations and experiment results. (a) Up-down movement, (b) roll and pitch angles during up-down flight, (c) flight in forward and backward directions, (d) roll and pitch during forward and backward flight, (e) left and right movement, (f) roll and pitch during left and right flight.

altitude. In **Figure 8b, d, and f** the body roll and pitch angles are drawn. It can be observed that angles ϕ and θ during simulation and experiments slightly differ. Therefore, we can conclude that the experimental results demonstrate the theoretical expectations.

4.2 Power line tracking simulation

In this section, simulation and experimental results during power line tracking are presented. The simulation setting is given in **Figure 9**. The simulation conditions are as follows:

- At the beginning of the simulation, the initial position of the UAV is 6 m above and 1 m on the port side of the power line.
- After position adjustment above the line for 10 s is done, the vehicle performs a wire tracking flight.
- The position of the power line in the vehicle coordinate system during tracking is set to $z = 3$ m and $y = 0$ m.

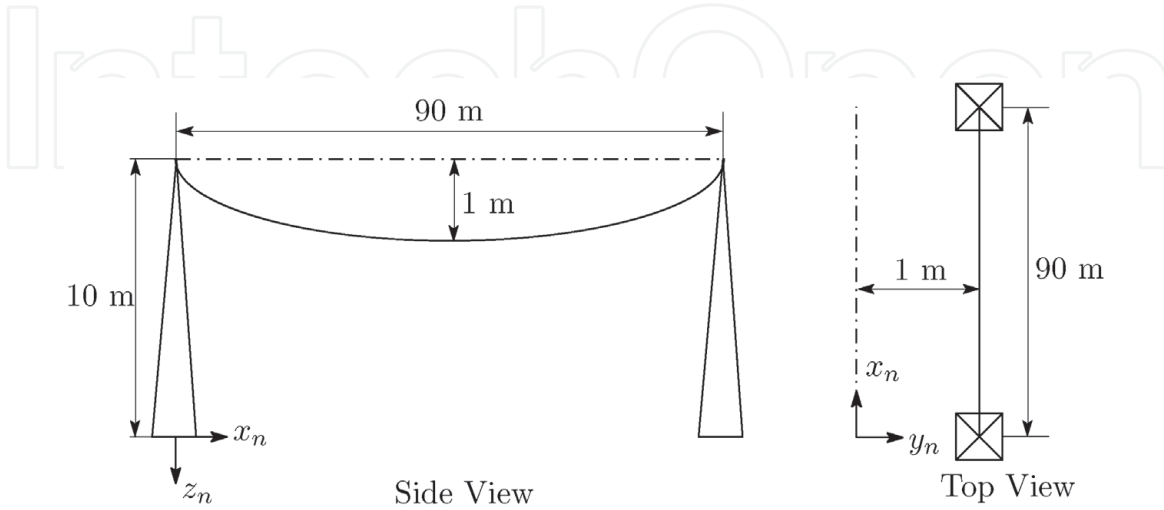


Figure 9.
Setup for power line tracking simulations and experiments.

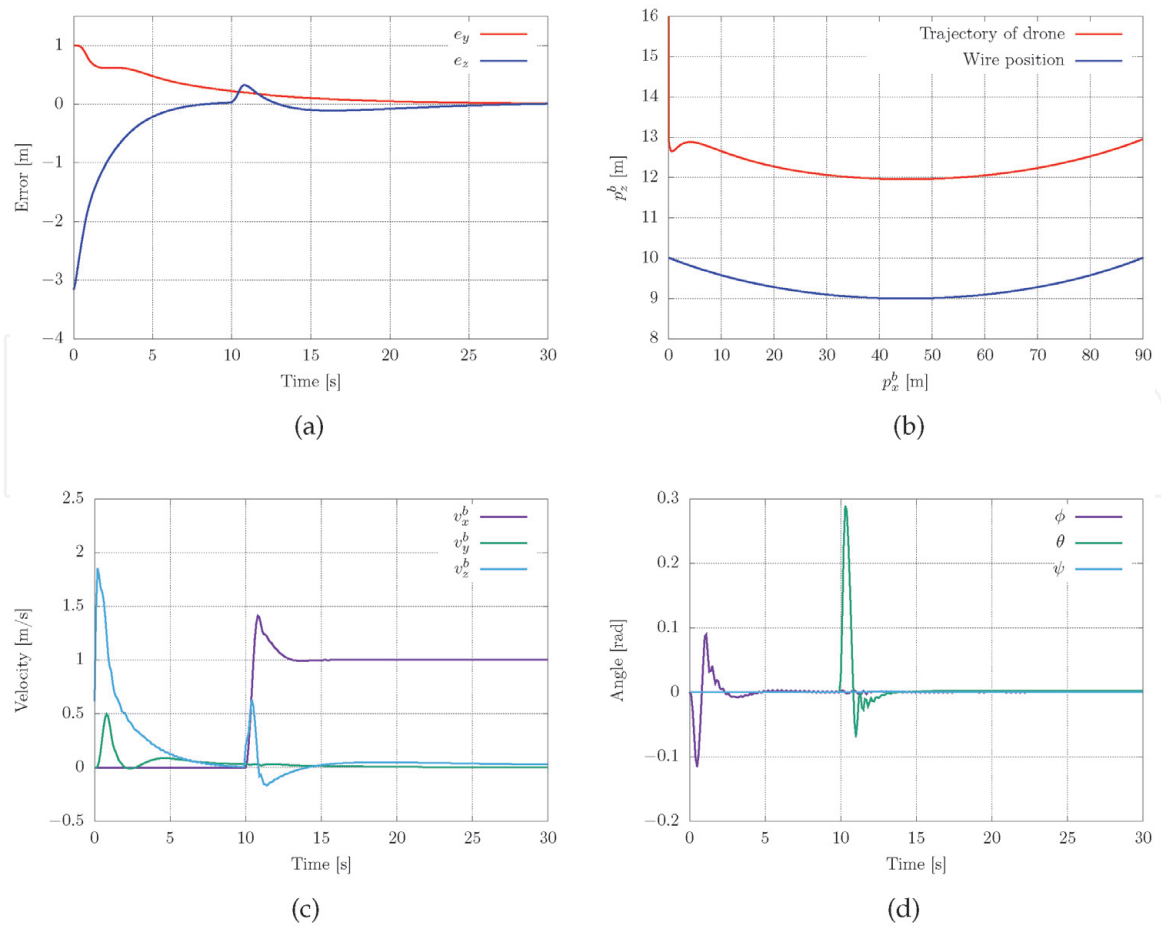


Figure 10.
Power line tracking simulation result. (a) Position error, (b) vehicle position vs power line, (c) vehicle speed, (d) roll and pitch body angles.

To achieve good performance during the simulation, the control frequency of inner loops is 400 Hz while the outer loops are at 10 Hz (see Section 2.2).

In the simulations, the catenary shape of the power line is expressed as:

$$w_z = \cosh(a_w(x_n - w_l/2)) + w_h, \quad (21)$$

where w_z is the vertical position of the power line in local coordinates, $w_l = 90$ is the distance between two towers the wire is attached to, and taking $a_w = 0.03$, $w_h = 8$ give a sag of 1 m with towers height of 10 m.

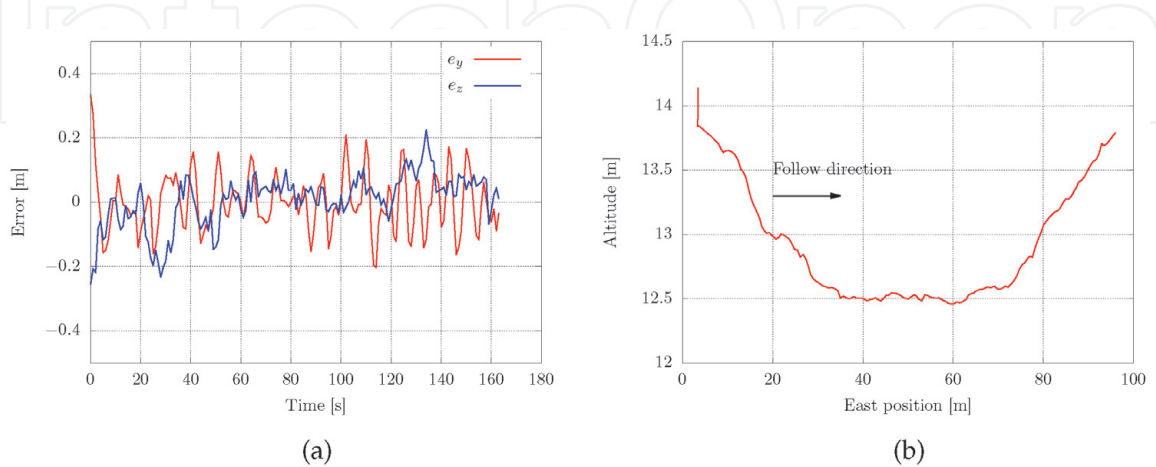


Figure 11. Ground wire tracking experiment. (a) Position error, (b) UAV path.

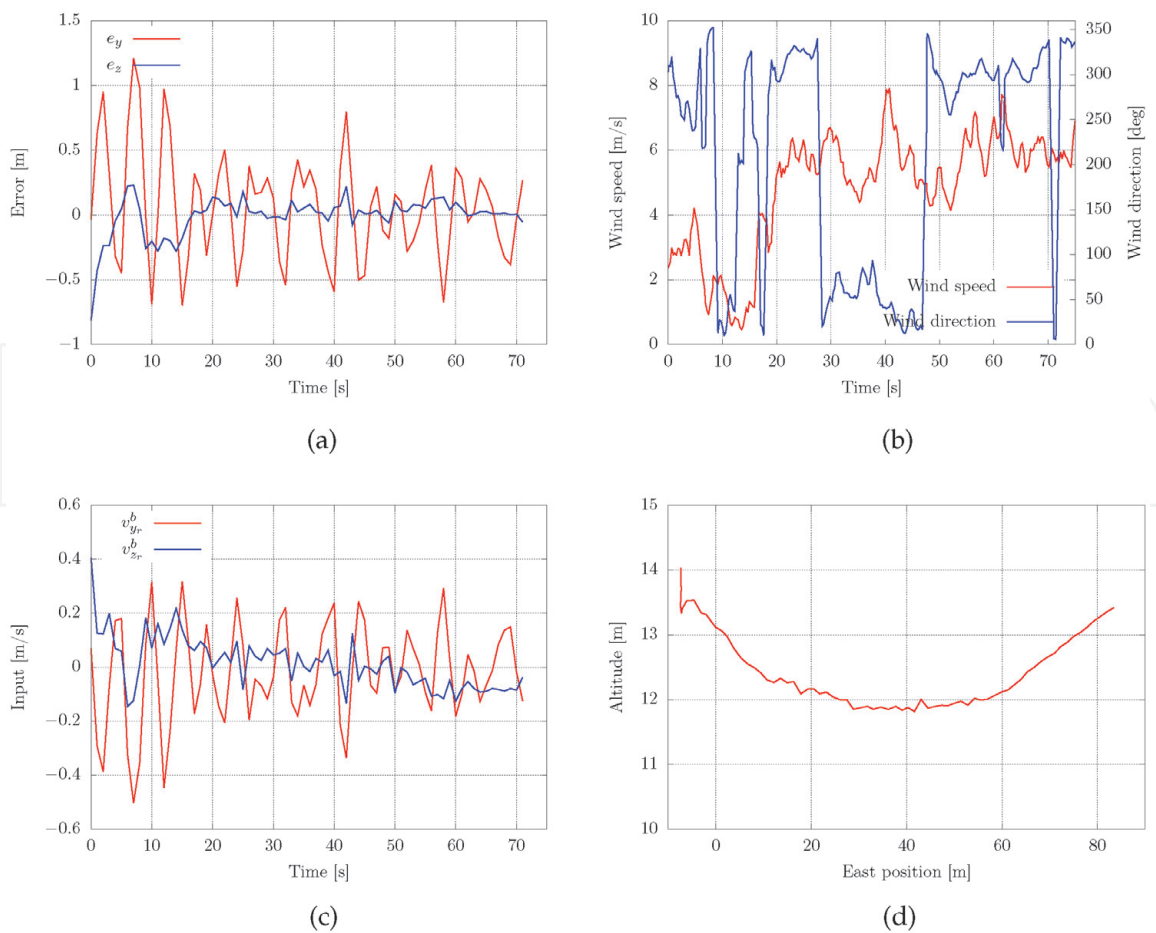


Figure 12. GW tracking experiment in presence of strong wind. (a) Position error, (b) wind speed and direction, (c) control input, (d) UAV path.

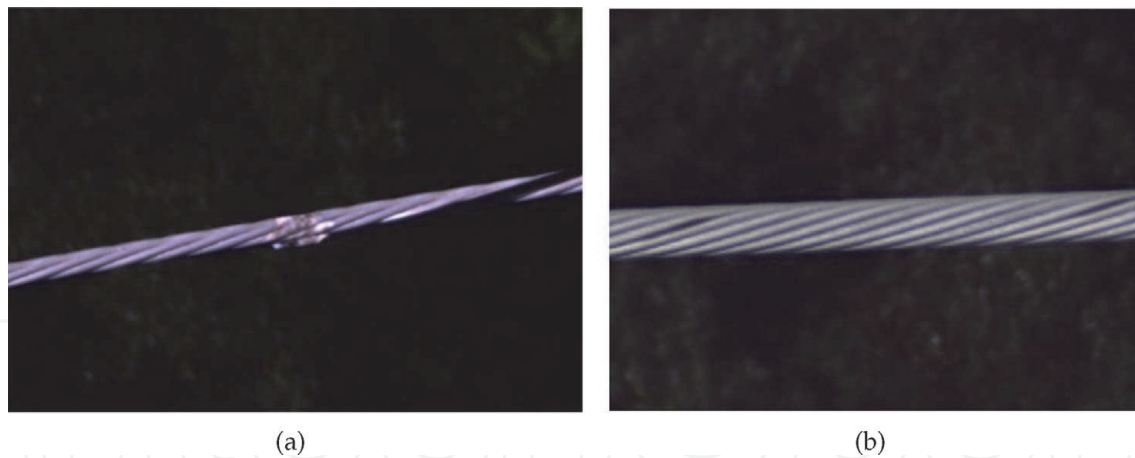


Figure 13. Images of ground wire. (a) Defect caused by a lightning strike. (b) Two minor defects.

Simulation results are shown in **Figure 10**. It can be seen from the same figure that the position error is negligible and converges quite fast.

4.3 Ground wire tracking experiment

In this section, the experimental results of actual ground line tracking flight are shown. The experimental setting is the same as the simulation one (see **Figure 9**). The diameter of the wire is 8 mm. The flights were performed autonomously, as explained in Section 3.3. The experimental results are shown in **Figures 11** and **12**.

The graphs in **Figure 11a** depict the position errors. The error in the vertical direction is less than ± 0.2 m and but the control quality is good. **Figure 11b** shows the vehicle trajectory—the catenary shape of the wire is well tracked. The vehicle speed was 0.7 m/s.

The graphs in **Figure 12** are taken in the presence of quite strong wind. It can be seen from the graph shown in **Figure 12a** that the position error in a vertical direction is small, but the error in the horizontal direction is about ± 0.5 m.

Figure 12b shows the wind speed and direction measured using an anemometer mounted on the vehicle body. The wind speed and direction are measured in 0.33 s interval, and graphs present 1 s average values. However, there were sudden changes in the wind speed up to 9 m/s. **Figure 12c** and **d** depict the control input and the catenary shape of vehicle trajectory. The vehicle speed in this experiment was 1.4 m/s.

Two images acquired during vehicle flight are depicted in **Figure 13**. Some minor defects can be observed there.

5. Conclusions

This work aims to develop a reliable autonomous power line tracking and inspection system based on a quadrotor helicopter. The model of the UAV was presented and evaluated in simulation and experiments performed in the real environment. Classical PID controllers were deployed, and their performances were demonstrated during ground wire line tracking. It can be concluded that the PID controller had a good performance, but in windy weather conditions, the position error increases to some extent. The presented system has almost Level 4 autonomy in the sense that it can perform flights beyond visual line of sight and without operator based navigation.

As a part of future work, we will implement a fuzzy PID controller to explore if further performance improvement can be achieved. This system will be implemented on regular inspections and maintenance of power facilities in an electric power company in Japan.

Acknowledgements

This research is performed in cooperation with Electric Power Development Co., LTD. from Tokyo, Japan. The authors would like to thank for their financial support of this project. We want to thank Mr. K. Tanaka, Mr. T. Sugiyama and Mr. Y. Oota from the same company for their help and support in performing most of the experiments.

Author details

Kenta Takaya^{1†}, Hiroshi Ohta^{2†}, Keishi Shibayama^{3†} and Valeri Kroumov^{2*†}

1 Graduate School, Okayama University of Science, Okayama, Japan

2 Okayama University of Science, Okayama, Japan

3 Scale Corporation, Asago City, Hyogo, Japan

*Address all correspondence to: val@ee.ous.ac.jp

† These authors contributed equally.

IntechOpen

© 2021 The Author(s). Licensee IntechOpen. This chapter is distributed under the terms of the Creative Commons Attribution License (<http://creativecommons.org/licenses/by/3.0>), which permits unrestricted use, distribution, and reproduction in any medium, provided the original work is properly cited. 

References

- [1] 60 Years Power Industry in Japan: Statistics. <https://www.fepc.or.jp/library/data/60tokei/index.html>, [Accessed: 02 Jul 2021], In Japanese.
- [2] Bian J., Hui X., Zhao X., and Tan M. A novel monocular-based navigation approach for uav autonomous transmission-line inspection. In *2018 IEEE/RSJ International Conference on Intelligent Robots and Systems (IROS)*, pages 1–7, 2018. doi: 10.1109/IROS.2018.8593926.
- [3] Yue L., Jun Y., Liang L., Jinlong Z., and Zongyu L. The method of insulator recognition based on deep learning. In *2016 4th International Conference on Applied Robotics for the Power Industry (CARPI)*, pages 1–5, 2016. doi: 10.1109/CARPI.2016.7745630.
- [4] Jabid T. and Uddin Md. Z. Rotation invariant power line insulator detection using local directional pattern and support vector machine. In *2016 International Conference on Innovations in Science, Engineering and Technology (ICISSET)*, pages 1–4, 2016. doi: 10.1109/ICISSET.2016.7856522.
- [5] Ohta H., Sato Y., Mori T., Takaya K., and Kroumov V. Image acquisition of power line transmission towers using uav and deep learning technique for insulators localization and recognition. In *2019 23rd International Conference on System Theory, Control and Computing (ICSTCC)*, pages 125–130, 2019. doi: 10.1109/ICSTCC.2019.8885695.
- [6] Zhai Y., Chen R., Yang Q., Li X., and Zhao Z. Insulator fault detection based on spatial morphological features of aerial images. *IEEE Access*, 6: 35316–35326, 2018. doi: 10.1109/ACCESS.2018.2846293.
- [7] Tao X., Zhang D., Wang Z., Liu X., Zhang H., and Xu D. Detection of power line insulator defects using aerial images analyzed with convolutional neural networks. *IEEE Transactions on Systems, Man, and Cybernetics: Systems*, 50(4):1486–1498, 2020. doi: 10.1109/TSMC.2018.2871750.
- [8] Jiang H., Qiu X., Chen J., Liu X., Miao X., and S. Zhuang. Insulator fault detection in aerial images based on ensemble learning with multi-level perception. *IEEE Access*, 7:61797–61810, 2019. doi: 10.1109/ACCESS.2019.2915985.
- [9] Luque-Vega L. F., Castillo-Toledo B., Loukianov A., and Gonzalez-Jimenez L. E. Power line inspection via an unmanned aerial system based on the quadrotor helicopter. In *MELECON 2014 – 2014 17th IEEE Mediterranean Electrotechnical Conference*, pages 393–397, 2014. doi: 10.1109/MELCON.2014.6820566.
- [10] Li Z., Liu Y., Hayward R., Zhang J., and Cai J. Knowledge-based power line detection for uav surveillance and inspection systems. In *2008 23rd International Conference Image and Vision Computing New Zealand*, pages 1–6, 2008. doi: 10.1109/IVCNZ.2008.4762118.
- [11] Zhou G., Yuan J., Yen I-L., and Bastani F. Robust real-time uav based power line detection and tracking. In *2016 IEEE International Conference on Image Processing (ICIP)*, pages 744–748, 2016. doi: 10.1109/ICIP.2016.7532456.
- [12] Golightly I. and Jones D. Visual control of an unmanned aerial vehicle for power line inspection. In *ICAR '05. Proceedings., 12th International Conference on Advanced Robotics, 2005.*, pages 288–295, 2005. doi: 10.1109/ICAR.2005.1507426.
- [13] Jones D., Golightly I., Roberts J., and Usher K. Modeling and control of a robotic power line inspection vehicle.

In *2006 IEEE Conference on Computer Aided Control System Design, 2006 IEEE International Conference on Control Applications, 2006 IEEE International Symposium on Intelligent Control*, pages 632–637, 2006. doi: 10.1109/CACSD-CCA-ISIC.2006.4776719.

[14] Feng T., Wang Y., and Zhu L. Power line recognition and tracking method for uavs inspection. In *2015 IEEE International Conference on Information and Automation*, pages 2136–2141, 2015. doi: 10.1109/ICInfA.2015.7279641.

[15] Chuang Deng, Jun-yong Liu, You-bo Liu, and Yang-yang Tan. Real time autonomous transmission line following system for quadrotor helicopters. In *2016 International Conference on Smart Grid and Clean Energy Technologies (ICSGCE)*, pages 61–64, 2016. doi: 10.1109/ICSGCE.2016.7876026.

[16] Araar O. and Aouf N. Visual servoing of a quadrotor uav for autonomous power lines inspection. In *22nd Mediterranean Conference on Control and Automation*, pages 1418–1424, 2014. doi: 10.1109/MED.2014.6961575.

[17] Valipour S., Khandani H., and Moradi H. The design and implementation of a hotline tracking uav. In *2015 3rd RSI International Conference on Robotics and Mechatronics (ICROM)*, pages 252–258, 2015. doi: 10.1109/ICRoM.2015.7367793.

[18] Pienroj P., Schönborn S., and Birke R. Exploring deep reinforcement learning for autonomous powerline tracking. In *IEEE INFOCOM 2019 - IEEE Conference on Computer Communications Workshops (INFOCOM WKSHPS)*, pages 496–501, 2019. doi: 10.1109/INFCOMW.2019.8845212.

[19] LineRanger : A Revolution in Transmission Line Robotics. <http://www.hydroquebec.com/robots/en/>, [Accessed: 08 Aug 2021].

[20] NYPA TESTS ROBOTIC TRANSMISSION INSPECTION TECHNOLOGY. <https://www.youtube.com/watch?v=DuKjnaiBP4c>, [Accessed: 08 Aug 2021].

[21] DJI – M200 Series– Powerline Inspection Tool. <https://www.youtube.com/watch?v=Bj5ByZKVNao>, [Accessed: 08 Aug 2021].

[22] Power Line Inspection Robot: Inspection Sample. <https://www.youtube.com/watch?v=cTPooHx6rr8>, [Accessed: 08 Aug 2021].

[23] Barker B. Robots take on tough tasks in transmission and distribution. *EPRI Journal*, pages 1–6, 02 2019.

[24] EPRI demonstrates autonomous drone. <https://www.neimagazine.com/features/featureepri-demonstrates-autonomous-drone-7967221/>, [Accessed: 08 Aug 2021].

[25] Explore the most dangerous places with autonomous drones. <https://www.exyn.com/>, [Accessed: 08 Aug 2021].

[26] Japan's first on-demand drone delivery service for hot lunches to healthcare professionals. <https://aeronext.com/news/yokosuka-beefbowldelivery/>, [Accessed: 08 Aug 2021].

[27] Takaya K., Ohta H., Kroumov V., Shibayama K., and Nakamura M. Development of uav system for autonomous power line inspection. In *2019 23rd International Conference on System Theory, Control and Computing (ICSTCC)*, pages 762–767, 2019. doi: 10.1109/ICSTCC.2019.8885596.

[28] Meyer J., Sendobry A., Kohlbrecher S., and Klingauf U. von Stryk O. Comprehensive simulation of quadrotor uavs using ros and gazebo. In *3rd Int. Conf. on Simulation, Modeling and Programming for Autonomous Robots (SIMPAR)*, pages 400–411, 2012. doi: 10.1007/978-3-642-34327-8_36.

- [29] Bouabdallah S. *Design and Control of quadrotors with application to autonomous flying*. PhD thesis, EPFL, Lausanne, 01 2007.
- [30] Hoffmann G., Waslander S., and Tomlin C. Quadrotor helicopter trajectory tracking control. In *AIAA Guidance, Navigation and Control Conference and Exhibit*, 2018. doi: 10.2514/6.2008-7410.
- [31] Dydek Z. T., Annaswamy A. M., and Lavretsky E. Adaptive control of quadrotor uavs: A design trade study with flight evaluations. *IEEE Transactions on Control Systems Technology*, 21(4):1400–1406, 2013. doi: 10.1109/TCST.2012.2200104.
- [32] Bouabdallah S., Noth A., and Siegwart R. Pid vs lq control techniques applied to an indoor micro quadrotor. In *Proceedings of 2004 IEEE/RSJ International Conference on Intelligent Robots and Systems*, volume 3, pages 2451 – 2456, 01 2004. ISBN 0-7803-8463-6. doi: 10.1109/IROS.2004.1389776.
- [33] PX4 Development Guide: PX4 Architectural Overview. <https://dev.px4.io/en/concept/architecture.html>, [Accessed: 04 May 2021].
- [34] Brescianini D., Hehn M., and D’Andrea R. Nonlinear quadrocopter attitude control. technical report. Technical report, EPFL, Zürich, 2013.
- [35] GPS for Yaw (aka Moving Baseline). <https://ardupilot.org/copter/docs/common-gps-for-yaw.html>, [Accessed: 07/06/2021].
- [36] Jetson-TX2 (Embedded computer). <https://developer.nvidia.com/embedded/jetson-tx2>, [Accessed: 04 May 2021].
- [37] MAVLink (Micro Air Vehicle Communication Protocol). <https://mavlink.io/en/>, [Accessed: 04 May 2021].
- [38] SkyHopper PRO. <https://www.skyhopper.biz/products/communication-data-links/>, [Accessed: 04 Jul 2021].
- [39] PixHawk (Flight Controller). <https://ardupilot.org/copter/docs/common-pixhawk-overview.html>, [Accessed: 04 May 2021].
- [40] ROS Kinetic Kame. <http://wiki.ros.org/kinetic>, [Accessed: 04 Jun 2021].